Unveiling the nature of giant radio galaxies

Dabhade, P.

6 | Chapter 6 : Barbell shaped giant radio galaxy with ~100 kpc kink in jet

We present here the study of a peculiar giant radio galaxy (GRG) - GRG-J2233+1315 using deep multi-frequency radio observations from GMRT and LOFAR along with optical spectroscopic observations with WHT 4.2m optical telescope. Our observations have firmly established its redshift of 0.09956 and unveiled its exceptional jet structure extending more than ~ 200 kpc culminating into a peculiar 'kink' structure of ~ 100 kpc. We measure the overall size of this GRG to be ~ 1.9 Mpc, which exhibits lobes without any prominent hotspots and closely resembles to a 'Barbell'. The magnetic field strength $\sim 5\,\mu$G and spectral ages of > 110 Myr for the radio lobes were estimated using high resolution radio data from LOFAR 144 MHz observations and GMRT 323 and 612 MHz observations. The deep low frequency radio maps also reveals many diffuse emission regions associated with the GRG. Despite its enormous size, the Barbell GRG is found to be residing in dense environment of either a small galaxy cluster or galaxy group. We discuss the possible causes for the 'kink' feature using various models of jet plasma instabilities.

P. Dabhade et al. 2021- A&A To be submitted

6.1 Introduction

Galaxies hosting active galactic nuclei (AGNs) which are strongly radiating at radio wavelengths are referred to as radio galaxies (RGs), which exhibit relativistic radio jets. Extended RGs with lobes (or edge-brightened) are categorised as Fanaroff-Riley type-II or FR-II (Fanaroff & Riley 1974) and the ones with centre-brightened features with bright jets and no lobe-hotspots are called the Fanaroff-Riley type-I or FR-I. This launching and propagation of jets is explained by the standard 'beam model' (Longair et al. 1973; Scheuer 1974; Blandford & Rees 1974), where collimated jets resulting from outflows originating from black holes, propel the extended structure. The dichotomy between the two classes of FR-I and FR-II type RGs is thought to be rooted in the AGN accretion mode and its connection with the jet power (Best & Heckman 2012a; Mingo et al. 2014; Hardcastle 2018a).

RGs extending to megaparsec (Mpc) scales are defined as giant radio galaxies (GRGs), which are quite rarer than RG population as shown in recent studies (Dabhade et al. 2020b,c). They are thought to be growing in the underdense environments and/or supplied with continuous jet power for a long duration ($\sim 10^8$ Myr), thereby allowing them to scale larger distances. Efforts to constrain models explaining the giant nature of GRGs are currently on-going (Gopal-Krishna et al. 1989; Subrahmanyan et al. 1996; Saripalli et al. 2005; Hardcastle et al. 2019; Dabhade et al. 2020c,a; Bruni et al. 2020). More discussion on the above can be found in Dabhade et al. (2020c).

The last few years has seen a resurgence in studies of GRGs owing to the new sensitive surveys at radio wavelengths like the LOFAR Two Metre Sky Survey (LoTSS; Shimwell et al. 2019), which is largely complemented by optical spectroscopic surveys like the Sloan Digital Sky Survey (SDSS; York et al. 2000; Abolfathi et al. 2018).

In the course of identifying giant radio galaxies and carrying out detailed multi-wavelength studies of GRGs under our project SAGAN* (Dabhade et al. 2017, 2020c), we have discovered a peculiar giant radio galaxy J223301+131502 (GRG-J2233+1315 for short form) from the NRAO VLA SKY SURVEY (NVSS; Condon et al. 1998) as reported in Dabhade et al. 2017. In this paper, we present our results on GRG-J2233+1315 based on optical and radio observations taken by us.

GRG-J2233+1315 is hosted by SDSS J223301.30+131502.5 galaxy, which exhibits a big diffuse stellar halo with apparent SDSS r-band magnitude (m_r) of 15.21 (Fig. 6.1). It has an elliptical morphology (Lintott et al. 2011) and has been classified to be of S0-a type galaxy (Paturel et al. 2003) with the isophotal diameter of (logd25) of 0.77±0.06. The stellar mass of the galaxy is $\sim 1.62 \times 10^{11}\,M_\odot$ (Lin et al. 2018).

It also has been identified as the brightest cluster galaxy (BCG) by MaxBCG Catalog of 13,823 Galaxy Clusters from the Sloan Digital Sky Survey (Koester et al. 2007) as MaxBCG338.25543+13.25070, GMBCG Galaxy Cluster Catalog of 55,424 Rich Clusters from SDSS DR7 (Hao et al. 2010) as J338.25544+13.25070,

*https://sites.google.com/site/anantasakyatta/sagan

and WHL cluster catalogue (Wen et al. 2012) of 132,684 clusters from SDSS-III data as WHLJ223301.3+131503. This is in contrast to the prevailing belief of GRGs residing in sparse environment (Mack et al. 1998; Subrahmanyan et al. 2008; Malarecki et al. 2015). Recently, large GRG samples from the LoTSS and NVSS have revealed more than 60 such examples of GRGs residing at the centres of galaxy clusters and groups (Dabhade et al. 2020b,c).

Earlier, Dabhade et al. 2017 used the photometric redshift (z) of ~ 0.093 from SDSS to estimate the total projected linear size of the GRG-J2233+1315 to be ~ 1.71 Mpc. Based on the only available radio data of NVSS at 1.4 GHz, Dabhade et al. 2017 observed a bright region possibly part of the GRG on the western side of the host galaxy and it was thought to be a 'knot' in the jet which is unresolved.

The important issue is to understand the growth and evolution of GRGs, which despite the dense environment manage to grow to megaparsec lengths. The combination of radio and X-ray data of such sources will enable us to study the inter-galactic medium (IGM) as well as the intra cluster medium (ICM). The interaction of the radio plasma with the hot ICM can possibly lead to the formation of 'cavities', which show up as depressions in the X-ray surface brightness maps (Bîrzan et al. 2004; McNamara et al. 2005). Research still continues on how these cavities influence the ICM as they could be supplying a dynamically important amount of heat and/or magnetic field to the ICM (Kronberg et al. 2001b; Quilis et al. 2001; Brüggen & Kaiser 2002; Fabian et al. 2002; Heinz et al. 2002; McNamara & Nulsen 2007). Hence, a GRG with nearly 2 Mpc size, residing in an over dense environment with peculiar radio morphology consisting of bright unresolved features and diffuse lobes warrants a detailed study using multi-frequency radio data.

6.2 Observations and data analysis

In this section we provide the details of the optical and radio observations and their corresponding data analysis for GRG-J2233+1315.

6.2.1 Optical

An accurate redshift of the GRG is needed to estimate its properties and hence, efforts were made to update the SDSS photometric redshift of 0.093 with spectroscopic observations. The optical spectrum of the host galaxy (SDSS J223301.30+131502.5) was obtained using the long-slit at 4.2m William Herschel Telescope (WHT), which is located at La Palma, Canary Islands. The observations were carried out on 27$^{\text{th}}$ June 2017 under the program id : W17AN014 using the Intermediate dispersion Spectrograph and Imaging System (ISIS*) instrument with a 3′ slit length and a slit width of 1.5″. Further details of the observations and data reduction are presented in section 2.2.1 of Saxena et al. (2019).

*http://www.ing.iac.es/astronomy/instruments/isis/index.html

We use the standard procedure of comparing the wavelengths of red-shifted lines (observed wavelengths) with the rest-frame emission and absorption lines as observed in Fig. 6.2 to estimate the redshift. We have used the standard IAU conversion from air to vacuum wavelengths (Morton 1991). The center, full width half maxima (FWHM) and error in FWHM for emission lines of the object, and the lamp spectra were measured using the Gaussian fitting routines. The instrumental broadening of grism 7 is 6.78Å. We have calculated the intrinsic FWHM using the instrumental broadening. We have calculated redshift from the observed wavelength and the error in redshift has been calculated using corrected FWHM. Using the corrected FWHM, we have also estimated stellar velocity dispersion (σ).

Table 6.1: Details of radio observations of GRG-J2233+1315 are provided in this table, where observations at 1280, 610, and 325 MHz are with GMRT and 144 MHz is with LOFAR. Primary calibrator refers to flux calibrator and secondary is the phase calibrator. Observation date format is dd/mm/yy. Project codes marked with * symbol are projects with co-observing scheme with the LoTSS.

Frequency (MHz)	Project Code	Observation Date	Obsid	Time on Source (mins)	Bandwidth MHz	Channels	Integration Time (secs)	Correlations	Primary Calibrator	Secondary Calibrator
(1)	(2)	(3)	(4)	(5)	(6)	(7)	(8)	(9)	(10)	(11)
1280	31_084	23/10/2016	8940	193	32	512	8	RR & LL	3C48	2148+069
612	28_020	17/05/2015	7785	225	32	512	8	RR & LL	3C48	2130+050
323	31_084	03/11/2016	8962	349	32	512	8	RR & LL	3C48	2212+018
144	LC6_024	05/09/2016	544937	480	49	231	1	RR & LL	3C196	3C196
144	LC11_009*	23/02/2019	695799	480	49	231	1	RR & LL	3C295	3C295
144	LC11_009*	11/05/2019	708070	480	49	231	1	RR & LL	3C295	3C295
144	LT10_010*	17/01/2020	765089	480	49	231	1	RR & LL	3C295	3C295
144	LT10_010*	26/03/2020	773699	480	49	231	1	RR & LL	3C295	3C295

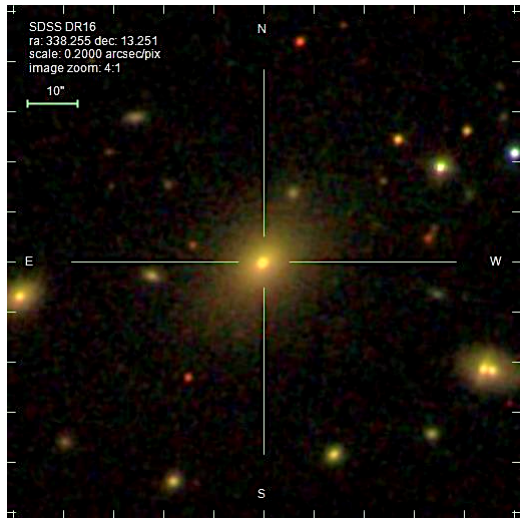

Figure 6.1: Multi-band colour composite optical image of SDSS J223301.30+131502.5 galaxy. The scales are given in the top left corner of the image.

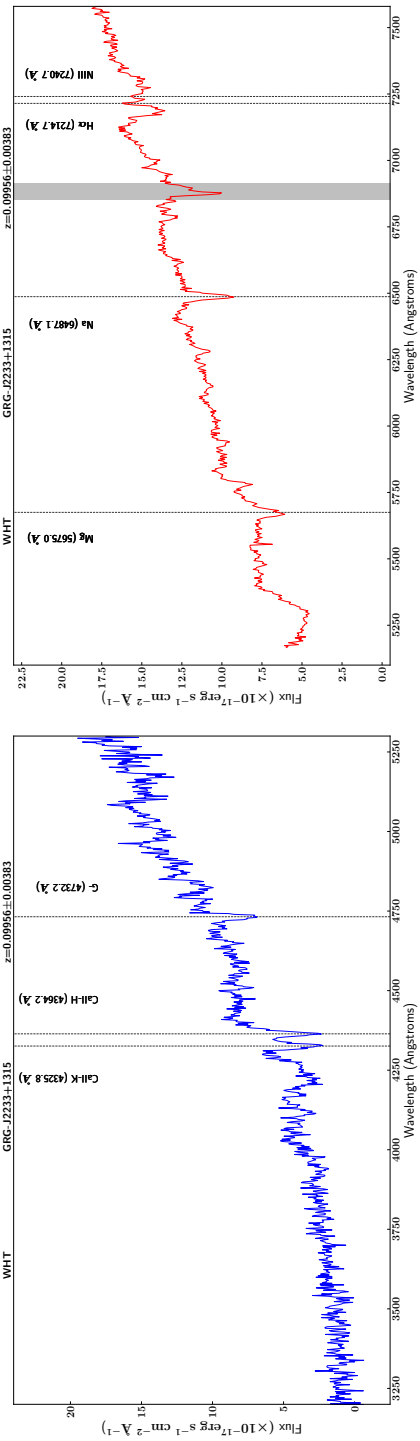

Figure 6.2: The plot shows 4.2m-WHT ISIS blue and red arm spectrum of the GRG-J2233+1315 in the shown wavelength ranges. The identified emission and absorption lines in the spectrum are marked with black dashed vertical lines. Spectrum from blue and red detectors are colour coded with their respective colours. The grey band represents telluric lines. More details can be seen in Sec. 6.2.1.

6.2.2 Radio Observations and data analysis

The GRG-J2233+1315 was observed (Tab. 6.1) at three frequencies with the Giant Metre-wave Radio Telescope (Swarup 1991; Swarup et al. 1991) covering the frequency range from ~300 to 1400 MHz. We obtained the coverage below 300 MHz with the LOw Frequency ARray's high band antennae (HBA) (van Haarlem et al. 2013). Below we describe the observations and data analysis.

GMRT observation and analysis

GRG-J2233+1315 was observed with GMRT in 2015-2016 at three frequencies as given in detail in Tab. 6.1 under the projects 28_20 and 31_84 (PI: Pratik Dabhade). The raw visibility GMRT data of all three frequencies was analysed using the Source Peeling and Atmospheric Modelling (SPAM; Intema et al. 2017) package. SPAM is based on the Astronomical Image Processing System (AIPS; Greisen 2003) and python programming language. To access tasks in AIPS, python based parseltongue interface (Kettenis et al. 2006) is used in SPAM. The analysis steps in SPAM starts with the flux and bandpass calibrations, which were derived from the respective calibrators after three cyclic iterations of flagging (Radio Frequency Interference-RFI) and calibrations based on models (e.g. Scaife & Heald 2012). In addition to the above, instrumental phase calibrations are also determined using methods of Intema et al. 2009. For ionospheric calibration, direction dependent gains are derived from the strong sources present in the field of view (FOV), which are then used to fit a time variable phase screen over the whole array. This phase screen is used later during imaging for correcting the entire FOV for effects caused by ionospheric phases. The derived calibrations were transferred to the target (GRG-J2233+1315) data. This was followed with imaging which consisted of several cyclic iterations of self-calibration with phase only gain calibration initially using local sky model derived from surveys like NVSS and others. The iterations also involved flagging of remaining weaker RFI. Finally, wide-field facet based imaging is carried out, with visibility weighting scheme of ROBUST -1 (AIPS) as it present a finer point spread function. Another three more iterations of self-calibrations were carried out with addition of amplitude calibration in the final round. In each round the process of peeling (Noordam 2004) was performed (see Intema et al. 2017 for details).

LOFAR observation and analysis

The GRG-J2233+1315 was observed three times between 2016-09 and 2020-03, once in a dedicated 8 hours LOFAR observation (project LC6_024, observation ID 544933, PI: Pratik Dabhade) and also as part of LoTSS where if we account for the target being offset from the pointing centre the effective integration time at the location of the target was also approximately 8 hrs (project LT10_010, co-observing project LC11_009 and observation IDs 695799, 708070, 765089, 773699). These observations were all conducted in HBA Dual Inner Mode and for this project we

made use of 231 0.195 MHz sub-bands between 120 and 169 MHz. Two 10 min calibrator observations were observed before and after each target observation. The basic details of these observations are summarised in Tab. 6.1.

The data were processed using the PreFactor pipeline* as described in van Weeren et al. (2016), Williams et al. (2016) and de Gasperin et al. (2019) which corrects the data for direction independent effects such as the bandpass, ionospheric Faraday rotation, clock offsets between different stations and an offset between XX and YY phases. The data were then processed with the latest version of the LoTSS direction dependent calibration pipeline, DDF-pipeline† which is summarised in Sec. 5.1 of Shimwell et al. (2019) and described in more detail in Tasse et al. 2020. This pipeline uses the calibration package kMS (Tasse 2014 and Smirnov & Tasse 2015) and imaging package DDFacet (Tasse et al. 2018) to perform a direction dependent self-calibration loop where calibration solutions are derived and gradually refined for 45 different directions spanning an $8° \times 8°$ field of view and applied during the imaging. After each individual pointing is imaged we used the procedure described in van Weeren et al. 2020 to refine the solutions in the direction of our target and allow for each re-imaging. For each pointing this involved subtracting sources away from the target region before phase shifting all datasets to be centred on the target and then performing a direction independent self calibration that makes use of WSClean (Offringa et al. 2014) and DPPP (van Diepen et al. 2018).

*https://github.com/lofar-astron/prefactor
†https://github.com/mhardcastle/ddf-pipeline

Table 6.2: Basic information about GRG. RA and Dec are Right Ascension and Declination of the host galaxy. S_ν is integrated flux density of the source and the P_ν is the radio power computed at frequency ν. $S_{1400MHz}$ is measured from NVSS. α_{int} is the integrated spectral index of the GRG from 144 MHz to 1400 MHz. Angular size refers to the largest angular size (LAS) of the GRG as measured from the radio maps. The flux density and corresponding power at 1300 MHz are from GMRT L-band observations. Here, $S_\nu \propto \nu^{-\alpha}$ convention is followed.

Properties	Values
RA	22 33 01.30
Dec	+13 15 02.52
r_{band} (mag)	15.04
Angular Size ($'$)	16.1
Redshift (z)	0.09956 ± 0.00383
Projected Size (Mpc)	1.83
$S^{Core}_{1300MHz}$ (mJy)	3.72 ± 0.84
$S_{1400MHz}$ (mJy)	231 ± 7.8
S_{612MHz} (mJy)	479 ± 24.3
S_{323MHz} (mJy)	835 ± 83.5
S_{144MHz} (mJy)	1487 ± 297.4
$P^{Core}_{1300MHz}$ ($\times 10^{22}$ W Hz^{-1})	9.30 ± 2.20
$P_{1400MHz}$ ($\times 10^{25}$ W Hz^{-1})	0.60 ± 0.05
P_{612MHz} ($\times 10^{25}$ W Hz^{-1})	1.3 ± 0.12
P_{323MHz} ($\times 10^{25}$ W Hz^{-1})	2.2 ± 0.30
P_{144MHz} ($\times 10^{25}$ W Hz^{-1})	3.9 ± 0.82
α^{1400}_{144}	0.82 ±0.18
Q_{Jet} (erg s^{-1})	1.3×10^{43}

Table 6.3: Radio properties of GRG-J2233+1315 as measured from our observations from GMRT and LOFAR along with archival NVSS data. EL and WL refer to the eastern and western lobes, respectively.

Region	$S_{1400MHz}$ (mJy)	$P_{1400MHz}$ $10^{24}WHz^{-1}$	S_{612MHz} (mJy)	P_{612MHz} $10^{25}WHz^{-1}$	S_{323MHz} (mJy)	P_{323MHz} $10^{25}WHz^{-1}$	S_{144MHz} (mJy)	P_{144MHz} $10^{25}WHz^{-1}$	α_{144}^{1400}
(1)	(2)	(3)	(4)	(5)	(6)	(7)	(8)	(9)	(10)
WL	30 ± 2.3	0.8 ± 0.08	90 ± 5	0.24 ± 0.02	177 ± 18	0.61 ± 0.03	344.3 ± 68.9	0.92 ± 0.20	1.07
EL	56.7 ± 3.1	1.5 ± 0.14	145.5 ± 7.8	0.39 ± 0.04	301.5 ± 30.3	0.80 ± 0.10	559.6 ± 112.1	1.49 ± 0.32	1.02

6.3 Results & Discussion

6.3.1 Redshift

The redshift (z) of GRG-J2233+1315 was found to be 0.09956 ± 0.00383 (Sec. 6.2.1). The observed spectrum (Fig. 6.2) lacks prominent emission lines and has detected absorption lines like Calcium H and K lines along with Magnesium and Sodium lines. Hence the galaxy appears to be a low-excitation GRG or LEGRG having old stellar populations. As discussed in Dabhade et al. 2020c the LEGRGs are the dominant population in comparison with the high excitation GRGs (HEGRGs).

6.3.2 Size, radio power and jet kinetic power

Using our radio observations with GMRT and LOFAR as described in Sec. 6.2.2, we obtained deep and high resolutions images at 1300, 612, 323, and 144 MHz as seen in Fig. 6.3. GMRT 323 MHz and LOFAR 144 MHz images are the deepest images showing the maximum extent of the source (largest angular size; LAS) of 16.1′, yielding a projected linear size of 1.83 Mpc. This has been computed with the formula given in Dabhade et al. 2020c and by using the cosmological parameters from Planck (H_0 = 67.8 km s^{-1} Mpc^{-1}, Ω_m = 0.308, Ω_Λ = 0.692; Planck Collaboration et al. 2016; scale at z=0.09956 is 1.896 kpc/″). We use the same parameters throughout the paper to estimate other properties.

In Tab. 6.2 we provide the measured and estimated properties of GRG-J2233+1315, where the total or integrated radio flux density and power are estimated in similar way as given in Dabhade et al. 2020c at various frequencies. At 1.4 GHz the total radio power of the GRG is $\sim 5\times 10^{24}$ W Hz^{-1}, which is somewhat on the lower side of GRGs as compared to typical radio powers of FR-II radio galaxies. Recent study of Mingo et al. 2019 has shown a population of low luminosity FR-II radio galaxies using LoTSS, which have radio powers below 10^{24} W Hz^{-1}.

The jet kinetic power has been estimated as per the scheme given by Hardcastle 2018b to be 1.4×10^{43} erg s^{-1}, which is not very high compared to very powerful FR-II radio galaxies and quasars which are usually above $\sim 10^{45}$ erg s^{-1} (Godfrey & Shabala 2013). As per figure 3 of Godfrey & Shabala 2013, GRG-J2233+1315 lies very close to the division between FR-I and FR-II type radio galaxies.

6.3.3 Radio morphology

Using the NVSS radio map of GRG-J2233+1315, Dabhade et al. 2017 reported a bright unresolved feature on the western side of the host galaxy, which was thought to be a knot in the jet. Now, with our deep and high resolution observations with GMRT and LOFAR, we have resolved the overall structure of the GRG-J2233+1315 in detail. Our multi-frequency radio maps from GMRT and LOFAR 144 MHz in Fig. 6.3, reveal a thin collimated jet emanating from the radio core

Table 6.4: Information of images shown in Fig. 6.3. The * symbol indicates high resolution image from LOFAR.

Image	Frequency (MHz)	RMS (mJy)	Resolution (″)
a	1300	0.013	2.5″ × 2.1″, 62.3°
b	612	0.039	7.1″ × 6.8″, 22.3°
Kink	612	0.031	5.1″ × 4.5″, 31.5°
c	323	0.081	12.1″ × 8.8″, 51.9°
d	144	0.242	20.0″ × 20.0″, 90.0°
d*	144	0.145	9.9″ × 5.5″, 80.9°

(detected only at 1300 MHz GMRT map) transforming into a ∼100 kpc 'omega' (**Ω**) shaped structure called the 'kink' on the western side. It is most likely that the 'kink' feature is also present on the eastern side in some form of symmetry. While the 'kink' on the western side of the jet is prominently seen, the 'kink' on the eastern side of the jet fails to show the same morphology. We suspect the 'kink' to be in different planes where only one of them is clearly observed due to projection effects. The radio images of all frequencies in our study show this highly complex and rare feature in the structure of the GRG. Beyond the **Ω** shaped 'kink' feature, the jet appears to re-collimate again having wider width than before and feed the mushroom shaped lobe. The two point sources embedded in the western lobe (Fig. 6.3 c) are unrelated sources and their flux densities were subtracted from the total flux density of the lobe.

Our highest resolution (2.5″ × 2.1″) radio map at 1300 MHz from GMRT reveals the radio core, which coincides with the galaxy called SDSS J223301.30+131502.5 and confirms its host nature. On the eastern side too we observe a twisted jet feature which eventually feeds the lobe. The jet terminating into the eastern lobe is fainter, possibly due to Doppler dimming, compared to the western side. The full jet connection to the lobe can be seen only in the GMRT 323 MHz and LOFAR 144 MHz maps. Interestingly, both the lobes are diffuse without any prominent hotspots, giving an impression of two buoyant bubbles being pushed out by the jets. Overall, the radio morphology of GRG-J2233+1315 resembles that of weight lifting equipment for exercises called the 'Barbell' (henceforth Barbell GRG).

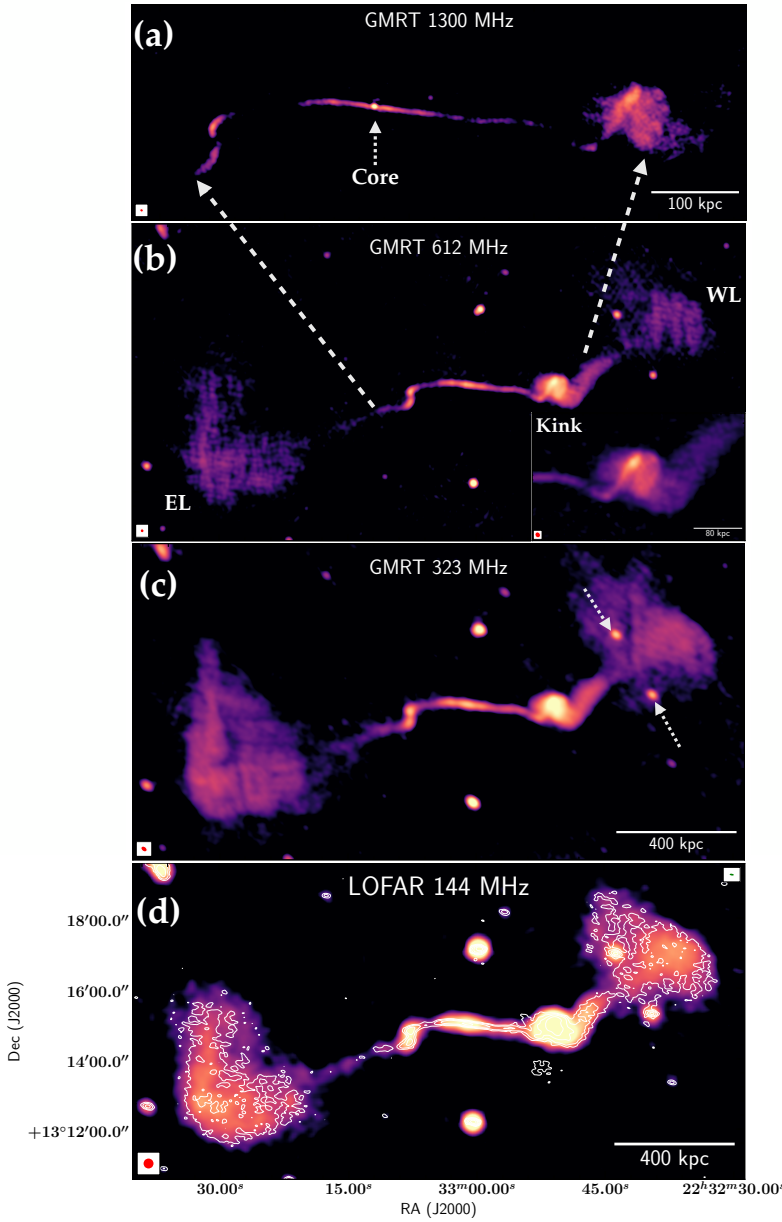

Figure 6.3: Radio images of GRG-J2233+1315 at 1300 (a), 612 (b), 323 (c) and 144 MHz (d) from top to bottom. The RMS and resolution information of respective images is provided in Tab. 6.4. The white box at bottom left represents the beam. In sub-image (b), additional zoom in image of the kink feature of the GRG is shown at the right bottom corner. The two arrows in sub-image (c) show two independent sources. In sub-image (d) LOFAR 144 MHz image is presented in two resolutions where the higher resolution is represented by contours, whose beam is shown on the top right corner of the sub-image.

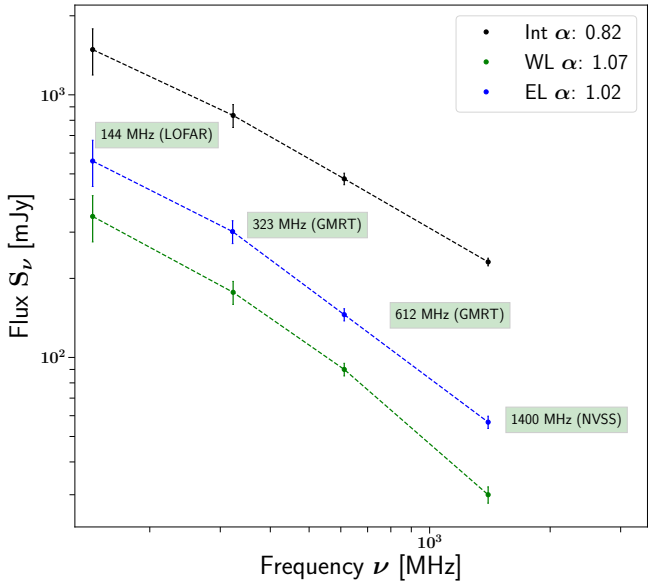

Figure 6.4: Spectral index plot of western (WL) and eastern (WL) lobes along with the full source (Int), where the 1400 MHz flux density was obtained from archival NVSS data. The possible break frequency is seen around ~ 323 MHz.

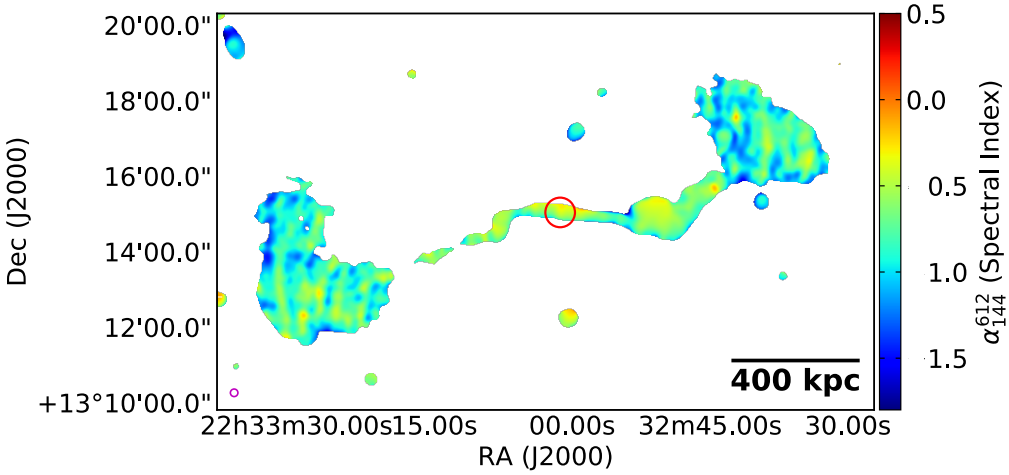

Figure 6.5: The figure shows the spectral index map made using LOFAR 144 MHz, GMRT 323 MHz and GMRT 612 MHz maps as described in Sec. 6.3.4. The red colour circular marker indicates the location of the radio core/host galaxy. The magenta colour circle at the bottom left represents the beam of 13″× 13″.

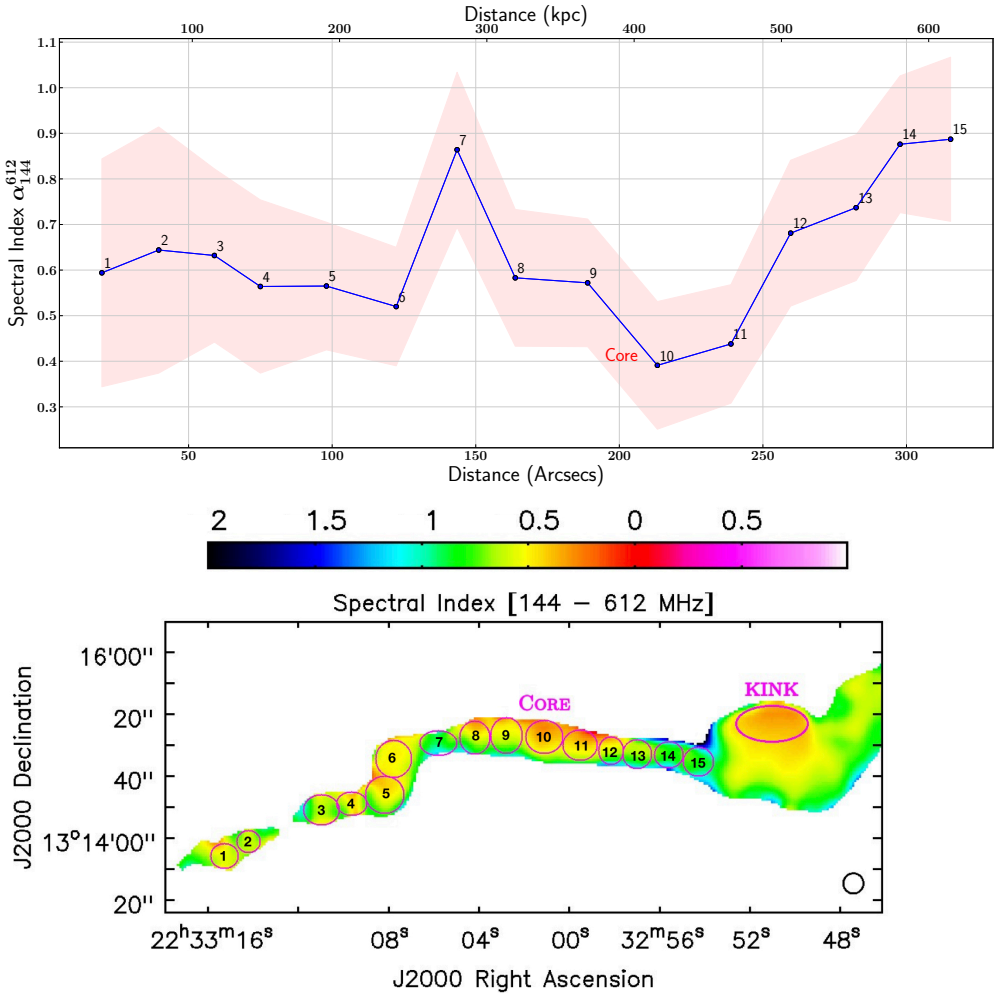

Figure 6.6: Upper figure shows the jet spectral index gradient with respect to distance as per the marked region seen in the lower plot. The shaded region indicates the uncertainties with the measurements. Lower figure zoomed in portion of Fig. 6.5 highlights the core, jet and the kink with numbered regions drawn on them.

6.3.4 Spectral index (α)

In Fig. 6.5 we see the three point spectral index map of the Barbell GRG made using LOFAR 144 MHz, GMRT 323 MHz and GMRT 612 MHz data at a resolution of 13″. Here, the frequency coverage on the higher side was restricted to 612 MHz due to lack of similar resolution maps at ∼1400 MHz which recover the entire source. The NVSS map with its coarser resolution of 45″ does not resolve the jets and 'kink' feature well, even though it does show the entire source emission. The other high frequency map available to us is from the GMRT 1300 MHz observation where the fine resolution and lack of short spacing do not recover the whole source. Therefore, in order to obtain high resolution spectral index information of the whole source, the NVSS and GMRT 1300 MHz data were not used.

The steps followed for making the three-frequency spectral index maps are based on the procedure given in Hoang et al. 2017. Firstly, the individual data sets (maps presented in Fig. 6.3) were further re-imaged with similar UV range ($0.2k\lambda$ to $50k\lambda$) and weighting schemes with uv-tapering to obtain maps at common resolution of 13″. From each map, only pixels with $\geqslant 3\times$ noise/RMS were used for the purpose of making spectral index calculation and map. The GMRT images were aligned with respect to the LOFAR image along with regridding all images to a common pixelisation. For the process of image aligning, we fitted compact point sources with 2D Gaussian function to find their accurate locations and average displacement thus was determined between the three images. Likewise, the GMRT images were appropriately shifted along the RA and Dec axes. The spectral index map as seen in Fig. 6.5 clearly shows flatness (∼0.5) of the radio core and the 'kink'. Both the lobes show steep (∼1) spectral index indicating older plasma.

6.3.5 Spectral ageing and magnetic field

One of the ways of estimating the life span of radio galaxies is through interpreting the radio spectrum ($S_\nu \propto \nu^{-\alpha}$) of their electron population, often known as the spectral age of the source. The shape of the spectra is highly influenced by two factors- the injection of energetic electrons and the electron population undergoing synchrotron and inverse-Compton losses. Energy losses for high energy electrons are indicated by a frequency break in the spectrum. It becomes steeper when the electrons are not rejuvenated due to the pause/end of AGN activity. The low-frequency (MHz) radio observations play an important role in determining the break (break frequency ; $\nu_{\rm br}$) in the power-law which occurs due to synchrotron losses. As more time elapses, the $\nu_{\rm br}$ moves to lower radio frequencies (Kardashev 1962; Pacholczyk 1970; Jaffe & Perola 1973). With the knowledge of break frequency and the magnetic field of the source, the spectral age can be calculated using the following formula :

$$\tau_{\rm sp} = 50.3 \left[\frac{\rm B^{0.5}}{(\rm B^2 + B_{IC}^2)} \frac{1}{[(1+z)\nu_{\rm br}]^{0.5}} \right] \tag{6.1}$$

where $B_{IC} = 3.25(1+z)^2$ is the magnetic field strength equivalent to the cosmic microwave background radiation and B is the magnetic field strength in various regions, which is expressed in μG . The term z is the redshift of the source and ν_{br} is the spectral break frequency in GHz above which the radio spectrum steepens from initial power-law spectrum. In the simple spectral ageing model, the magnetic field is assumed to be constant in a given region throughout the energy loss process. Also, it is assumed that there is no energy loss due to expansion process and the particles have a constant power law energy spectrum. To determine the spectral ages of eastern lobe (EL) and western lobe (WL) of the Barbell GRG, a cylindrical geometry is assumed, and the sizes (d) of the specified regions are computed from the lowest frequency map of LOFAR 144 MHz. The magnetic fields in the corresponding regions are calculated using both classical (Miley 1980) and revised (Beck & Krause 2005) formalism by assuming minimum energy conditions. The following formulae have been used for calculations :

$$u_{\min}\left[\frac{\text{erg}}{\text{cm}^3}\right] = \xi(\alpha,\nu_1,\nu_2)(1+k)^{4/7}(\nu_0\,[\text{MHz}])^{-4\alpha/7} \times (1+z)^{(12-4\alpha)/7}\left(I_0\,[\frac{\text{mJy}}{\text{arcsec}^2}]\right)^{4/7}(d\,[\text{kpc}])^{-4/7} \tag{6.2}$$

$$B_{\text{eq}}[\text{G}] = \left(\frac{24\pi}{7}\,u_{\min}\right)^{1/2}, \tag{6.3}$$

$$\text{B}'_{\text{eq[G]}} \sim 1.1\gamma_{\min}^{\frac{1-2\alpha}{3+\alpha}} \times \text{B}_{\text{eq}}^{\frac{7}{2(3+\alpha)}}. \tag{6.4}$$

Assuming a uniform magnetic field and an isotropic particle distribution, the minimum energy density ($u_{\min}$) is computed, where the parameter ξ is a function of spectral index α. Different values of ξ are taken from Table 1 in Govoni & Feretti 2004. In classical formalism, the spectrum is integrated from ν_1 to ν_2, usually from 10 MHz to 100 GHz, which corresponds to a minimum Lorentz factor (γ_{min}) of $\approx$ 10 and a maximum Lorentz factor (γ_{max}) of $\approx 10^4 - 10^5$ respectively. k represents ratio of energies in relativistic protons to electrons (1 or 100), I_0 is the surface brightness at the measuring frequency and d is the mean of major and minor axis (source depth). Also we assume the filling factor to be 1. The terms B_{eq} and B'_{eq} represent the classical and revised equipartition magnetic fields, respectively, which are related to $u_{\min}$ as seen in equation 6.3.

Based on our analysis, the equivalent magnetic field of the lobes is around 5μG (Tab. 6.5) which is similar to that of other GRGs (Ishwara-Chandra & Saikia 1999; Konar et al. 2004; Kronberg et al. 2004; Harwood et al. 2016). Also, when compared with RGs of similar radio power and located in galaxy cluster centres from Bîrzan et al. 2008 sample, the magnetic filed strengths are comparable. It has been suggested that powerful radio galaxies, especially GRGs covering Mpc scale volumes are strong candidates for magnetising the intergalactic medium (Rees 1987; Ruzmaikin et al. 1989; Jafelice & Opher 1992; Kronberg 1994; Kronberg et al. 2001b). This largely depends on how powerful the RG/GRG is along with its environment and hence, its direct effect may vary as per the source. A study

by Jafelice & Opher 1992 of modelling powerful radio galaxies (e.g. M84, 3C 465, and NGC 6251) based on observations have estimated the inter-galactic medium magnetic fields to be in the range of $10^{-6} - 10^{-10}$ G.

Considering synchrotron radiation mechanism in which the electrons are losing energy, the spectral ages are defined to be the time progressed since the acceleration of the particles. In addition to the above mentioned radiative cooling losses, the depletion in particle and field energy in the radio lobe can also be caused due to adiabatic expansion (Scheuer & Williams 1968). This can lead to reduction in magnetic field and break frequency, causing the measured spectral age to surpass the actual age of the radio source. Our results for the spectral ages of the Barbell GRG are presented in Tab. 6.5, where adopting the commonly used k-value of 1, spectral ages of >110 Myr have been obtained for the radio lobes. To match the spectral age with the dynamical age, the jet head speed would need to be as low as ~ 0.03c (considering distance between the radio core and western lobe). The spectral age estimation suffers from some uncertainties like inhomogeneity in magnetic field and lack of accurate injection index values. It is often found (Machalski et al. 2009) that the spectral age differs from the dynamical age of the source which mainly depends on the geometry and brightness of the radio source.

The spectral ages of the both the lobes for the Barbell GRG are quite on the higher side as compared to RGs, however past studies of GRGs on spectral ageing have yielded wide range of values between ~ 10 Myr to 250 Myr (Mack et al. 1998; Schoenmakers et al. 2000b; Konar et al. 2004, 2008; Jamrozy et al. 2008; Shulevski et al. 2019; Cantwell et al. 2020). It is worth noting that the method for estimating spectral ages was not uniform across all the above mentioned spectral ageing work on GRGs.

Table 6.5: Values of Equipartition Magnetic Field and Spectral Age estimated for the entire source as described in Sec. 6.3.5. The assumed break Frequency (ν_b) is 323 MHz. Terms with (cl) are from classical formalism and the ones with (rev) are using revised formalism of Beck & Krause 2005.

Region	K-value	α	d	u_{min}	B_{eq}(cl)	B'_{eq}(rev)	(ν_b)	τ_{sp}(cl)	τ_{sp}(rev)
			kpc	$\times 10^{-12}$ (erg cm^{-3})	(μG)	(μG)	(MHz)	(Myr)	(Myr)
WL	1	1.07	520	1.30	3.8	6.7	323	175	115
	100	1.07	520	0.13	11.7	17.4	323	60	35
EL	1	1.02	610	1.05	3.4	5.7	323	185	133
	100	1.02	610	9.80	10.3	15.2	323	70	42

6.3.6 Jet and the kink

The Barbell GRG shows a remarkable long collimated jet of $\sim 113''$ in length corresponding to ~ 210 kpc (projected). A very few radio galaxies have shown long collimated jets extending to hundreds (> 200 kpc) of kpc, e.g. NGC 315 and HB13 (Jaegers 1987), CGCG 049-033 (Bagchi et al. 2007), and 4C 34.47 (Hocuk & Barthel 2010). However, unlike these sources, the Barbell GRG exhibits a counter jet on the eastern side, which is rare in GRGs with FR-II type morphology. In subfigure (c) and (d) of Fig. 6.3, we clearly see the counter jet feeding the eastern lobe. The projected length from eastern lobe to the prominent 'kink' on the western side exceeds ~ 400 kpc in length. Since the Barbell GRG is not residing in an underdense environment, it must be possessing a very energetic jet powered by a SMBH of the host BCG.

There are many similarities between the Barbell GRG and NGC 6251, which is also a ~ 2 Mpc GRG residing in a relatively denser environment with a ~ 200 kpc one sided (north-western) jet (Waggett et al. 1977). This jet dubbed as the 'blow-torch jet' has been a subject of several studies (e.g. Perley et al. 1984; Mack et al. 1997; Evans et al. 2005b) ranging from radio to X-rays wavelengths. A counter-jet of ~ 50 kpc was detected by Perley et al. 1984 using VLA and recently, better maps showing extended jet emission by Cantwell et al. 2020 using LOFAR and VLA were presented. The spectral ages (~ 200 Myr) too are similar for both NGC 6251 (Cantwell et al. 2020) and Barbell GRG, which are on the older side compared to some other GRGs.

In Fig. 6.6, we show the spectral index (α) gradient along the jet and the counter-jet which ranges from ~ 0.6 to 0.9, which is quite similar to that of the jet in NCG 6251 as presented by Perley et al. 1984. The radio jets produced near to the central super-massive black holes are collimated by magnetic field and their collimation require external confinement (Tomimatsu 1994; Beskin et al. 1998). For the external confinement, the gas pressure profile plays a vital role and hence, influences the jet acceleration and collimation along with the magnetic field configuration. For the jet in GRG NGC 6251, Perley et al. 1984 have discussed a model for jet confinement at large scales due to thermal pressure of the environment and how its non-uniformity can affect the overall source morphology. Hence, in Barbell GRG it is interesting to see ~ 280 kpc collimated jet propagating in low mass galaxy cluster environment with weak X-ray emission (no detection in ROentgen SATellite or ROSAT sky survey). In absence of the gas pressure profile of this dense environment it is not possible to model the parameters of the jet.

Gower et al. 1982 presented a simple yet effective kinematical model of precessing twin jets with relativistic bulk velocity which explained peculiar radio jets with twists and turns of several radio galaxies and quasars. Parts of the Barbell GRG resemble that of the radio galaxy 3C 449, whose peculiar jet morphology with mirror symmetry has been explained by Gower & Hutchings 1982 with a simple precessing beam model having relativistic bulk motion. The precessing jets model is required to be explored further in detail to explain aspects of the complex jet and 'kink' morphology in the Barbell GRG.

The Magnetohydrodynamic (MHD) processes govern the launch, acceleration and collimation of astrophysical jets. Several works (Hummel et al. 1992; Baum et al. 1997; Feretti et al. 1999; Lobanov & Zensus 2001; Marshall et al. 2001; Mertens et al. 2016) in the past three decades have shown the presence of peculiar features in the jets on sub-parsec to kpc scales, which appear to be wiggles or 'kinks'. However, almost all of them are on smaller scales (~ 10 kpc), and not scales of ~100 kpc as in the case of 'kink' in the Barbell GRG. The ~ 100 kpc omega shaped 'kink' structure seen on the western side of the radio core is the only one known, and an unique example of plasma instability on such large scale. As discussed previously in Sec. 6.3.3, there is a possibility that eastern side also harbours a 'kink' but is not visible due to possible projection effects. However, we do see flat spectral index (though as not as flat as on the western side) near the twisted part of the jet on the eastern side, which is marked with six numbered circles in Fig. 6.6. Below, we will discuss the 'kink' feature of the Barbell GRG based on the clearly observed one on the western side and its possible causes.

The radio jets are susceptible to Kelvin-Helmholtz (KH) instabilities when they encounter ambient medium with contrasting densities and flows (Birkinshaw 1991; Hardee 2007; Perucho et al. 2007). The environment in which the Barbell GRG is residing, most certainly provides ideal conditions for development of KH instabilities and the observed 'kink' feature could possibly be its manifestation in some form.

Another possibility is that the observed 'kink' feature in the Barbell GRG could also be the site for possible magnetic reconnection (Romanova & Lovelace 1992), where the brightening in the jet is observed. This bright or excess emission in the jet can be explained by magnetic reconnection rather than shocks (Sironi et al. 2015) as it has been shown via simulations that shocks while efficiently dissipating energy, do not accelerate particles much above the thermal energy. Recent observation based studies (Shukla & Mannheim 2020; Meyer et al. 2020) also have shown compelling evidence of magnetic reconnection in jets of AGNs using high energy instruments, however these are on much smaller scale as well as closer to the AGN.

The current-driven (CD) 'kink' or shear-flow instability can also cause the jets to be unstable and often lead to brightening in regions of the jets Chiuderi et al. 1989; Nakamura & Meier 2004. Using three-dimensional MHD simulations, Nakamura & Meier 2004; Nakamura et al. 2007 have proposed that the main reason for the observed wiggles or 'kink' features in jets is due to CD instability. In this type of instability, a helical structure is developed with a relatively low growth rate. Simulation studies by Mizuno et al. 2009, 2012, 2014 have shown that CD instability can stimulate large-scale helical motions in the jets leading to deformation and but need not disrupt the jet completely. Here, the distorted magnetic field structure can possibly prompt the creation of magnetic reconnection. Their simulations also revealed that the CD instability mainly depends strongly on the magnetic pitch profile and moderately on the density profile. Also, the velocity shear radius relative to the characteristic radius of the magnetic field determined

the static and non-static feature of the 'kink'. In case of Barbell GRG we observe the jet on the western side to develop 'kink' like feature and again recollimating to feed the western lobe.

High resolution studies of radio AGN using Very Long Baseline Arrays are extremely important for studying jets as they allow us to peer close to the region of jet launching. Using multi-epoch VLBA observations at 15 GHz for BL Lacertae (BL Lac), Cohen et al. 2015 have shown a strong possibility of detecting Alfvén waves propagating in the radio jet emanating from the black hole. Their observations have shown the existence of a strong transverse component of the magnetic field belonging to the BL Lac's jet. Assuming the magnetic field to be helical based on previous observational studies (Gabuzda et al. 2004), they suggest that the observed features in the BL Lac are due to transverse S (shear) Alfvén waves propagating along with longitudinal component of the magnetic field. These Alfvén waves appear to be stimulated by changes in the position angle of the recollimation shock, which is analogous to a 'whip'* in action. Currently, it is unclear whether such disturbances along with jets can propagate to larger scales but the above study does certainly draw some similarities to that of the observed peculiar 'kink' feature in the Barbell GRG.

An interesting mechanism is proposed by Nakamura et al. 2001 using helical kink instability to explain the observed 'wiggles' or 'kink' features in radio jets of AGNs. It is based on the 'Sweeping Magnetic-Twist' model, which conjectures that the AGN core provides the necessary large amount of energy required for producing systematic magnetic configuration. Their simulations conclude that the most optimum mode of carrying this energy is via the Poynting flux of torsional Alfvén wave train (TAWT), which is produced by interaction of rotating accretion disk of the AGN and the large scale magnetic field. The observed 'wiggles' or 'kink' then can arise from MHD processes under the influence of TAWT which when encounters low Alfvén velocity, creates a pinched region and other deformations in the jet. Unlike the previously discussed models above, this model explains distortions in jets on larger scale, as the magnetic twist cannot be created at large distances locally, the TWAT can come along the jet from the radio core of the AGN.

The brightest part of the Barbell GRG is the 'kink' feature, which is possibly the working surface of supersonic jets in which the bulk kinetic energy is abruptly dissipated within decelerating shock waves. At the location of the shock fronts formed in the jets, the relativistic electrons are efficiently accelerated due to the impact with the ambient surrounding medium. This is evident from the flat spectral index (0.38) of the top of the 'kink' feature' as seen in the lower figure of Fig. 6.6. The 'kink' feature could also be due to the flow of plasma along a bent magnetic field.

Assuming the region highlighted in ellipse in the lower figure of Fig. 6.6 to represent a shock front, we attempt to estimate its mach number using diffusive shock acceleration (DSA) mechanism (Blandford & Eichler 1987), where

*link

$$\alpha_{\rm inj} = -\frac{1}{2}\left(\frac{1+3/\mathcal{M}^2}{1-1/\mathcal{M}^2}\right). \tag{6.5}$$

The radiative losses of electrons will lead to steepening of the radio spectrum and upon integrating over larger frequency range, the spectral index of the integrated power law will take the form-

$$\alpha_{\rm int} = \alpha_{\rm inj} - 0.5 = -\left(\frac{1+1/\mathcal{M}^2}{1-1/\mathcal{M}^2}\right). \tag{6.6}$$

The integrated spectral index $\alpha_{\rm int}$ at the top of the 'kink' feature as marked with an ellipse in Fig. 6.6 (top) is $\sim$0.38. Using the $\alpha_{\rm int}$ value and the Eq. 6.6, the mach number ($\mathcal{M}$) of the possible shock front is $\sim$1.5, which is not very high. However, jets with relativistic plasma which are magnetically dominated are not efficient sites for shock acceleration (Sironi et al. 2013, 2015). Hence, the magnetic reconnection explanation for the observed brightening in the 'kink' seems plausible.

6.3.7 Environment Studies

It is essential to study the environment of GRGs as one of the most favoured explanation for their gigantic sizes is attributed to their under-dense environment (Mack et al. 1998). Another important reason to study their environment is to understand its effect on their morphologies. Some GRG studies (Schoenmakers et al. 2000b; Lara et al. 2001a; Subrahmanyan et al. 2008; Pirya et al. 2012) have indicated that the observed asymmetries in the morphologies of the GRGs trace the asymmetries in their environment. Hence, GRGs with their large sizes become a natural probe of environment asymmetries over megaparsec scales (Subrahmanyan et al. 2008; Safouris et al. 2009). In the case of Barbell GRG which resides in a relatively denser environment, we do observe asymmetries in its jets which possibly could be due to their immediate environments.

GRGs hosted by BCGs in cluster environment are quite rare, and as shown by Dabhade et al. 2020c, less than 10% of the known GRG population are BCGs. Using information from Wen et al. 2012, we have estimated the following information about the galaxy cluster in which GRG-J2233+1315 resides (Fig. 6.7)-
$\mathbf{R_{200}}$ =1.02 Mpc (virial radius of the galaxy cluster)
$\mathbf{R_*}$ = 20.04 (richness of the galaxy cluster)
$\mathbf{N_{200}}$ =13 (No. of galaxies observed within $\mathbf{R_{200}}$)
$\mathbf{M_{200}} = 1.1 \times 10^{14}\ \mathbf{M_\odot}$ (Mass within $\mathbf{R_{200}}$)
Volume = 4.4 $\mathbf{Mpc^3}$ (Volume of cluster within $\mathbf{R_{200}}$)
Density = $2.4 \times 10^{13}\ \mathbf{M_\odot}$ / $\mathbf{Mpc^3}$
$\mathbf{L_x} = 3 \times 10^{43}$ erg s^{-1} (Cluster X-ray luminosity)
$\mathbf{T_x}$ = 2.3 KeV [X-ray band - 0.1 to 2.4 KeV]

The mass ($\mathbf{M_{200}}$) of the galaxy cluster reflects that it is either a low mass galaxy cluster or a massive galaxy group. Also, based on the available information, it was

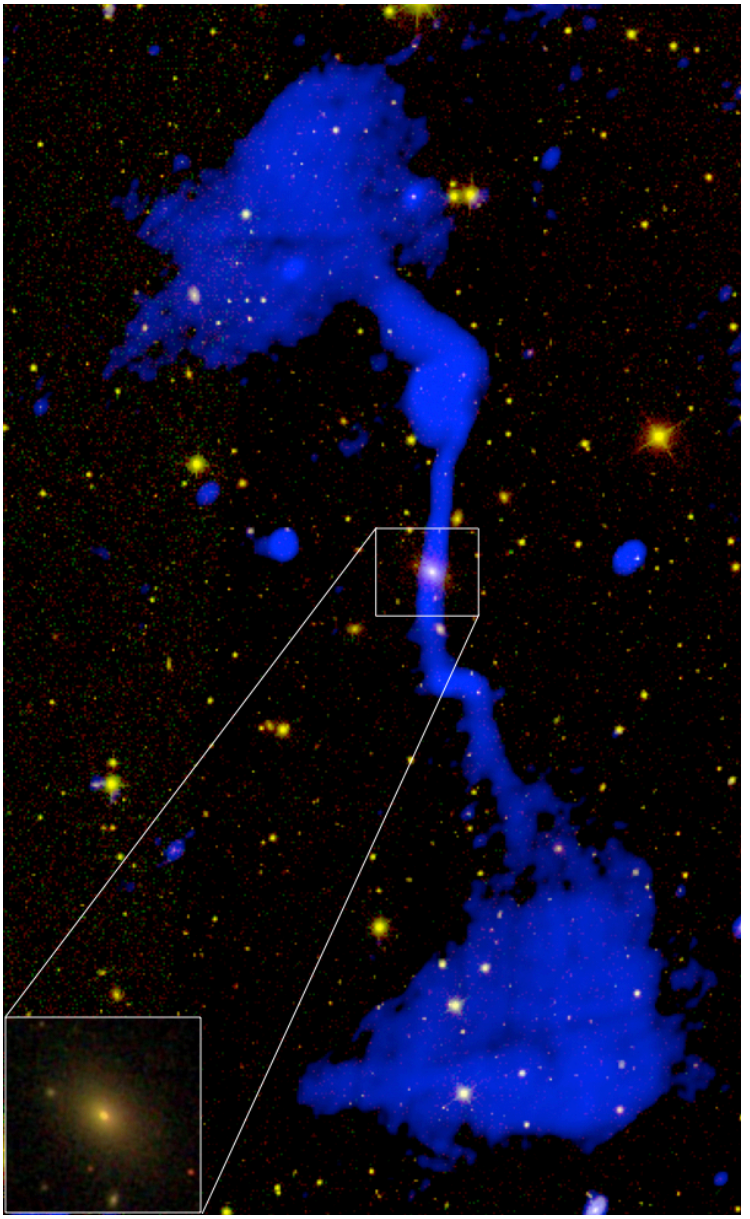

Figure 6.7: Optical and radio colour composite image where the background yellow colour image represents SDSS and the blue represents radio emission as seen in GMRT 325 MHz map. At the top left a zoom in view of the host galaxy i.e., the BCG is shown.

shown that GRGs do not reside in centres of very massive clusters Dabhade et al. 2020c. If R_{200} is indeed ~1.02 Mpc, then the GRG-J2233+1315 lies within the virial radius of the galaxy cluster. If R_{200} is lower than 1.02 Mpc then the lobes can possibly be located at the edge of R_{200} or beyond, where thermal pressure from external medium for confining the radio lobes will be less and thereby allowing free adiabatic expansion. Hence their expansion dynamics will be governed by inter-galactic medium and will possibly move in the direction of low pressure gradient due to buoyancy.

As seen above, the Barbell GRG resides in relatively low mass cluster and the lack of detection in the ROSAT sky survey supports the finding. Hence, it can be said that with the right combination of kinetic jet power and the ambient medium, the collimated jet has been able to travel to large distance unhindered until developing the 'kink'. Based on the observed peculiar morphology of the GRG, it is apparent that environment certainly has influenced its growth. Further deep optical spectroscopic data of surrounding galaxies and X-ray data of the galaxy group/cluster will be needed to explore its exact dynamics.

6.4 Summary

We have presented our study on a ~ 1.9 Mpc large GRG called the Barbell GRG, which is hosted in a dense cluster/group environment. Our optical spectroscopic data from WHT has established the redshift of the GRG and hence, its projected linear size. Our deep and high resolution radio images from GMRT and LOFAR reveal a ~ 210 kpc jet emanating from the radio core and leading to ~ 100 kpc 'kink' structure possibly caused due to some form of instability. Our multi-frequency radio data has enabled us to estimate the magnetic field and spectral ages of the diffuse lobes. The classical equivalent magnetic field of the lobes is $\sim 5\,\mu$G and the spectral ages of ~ 180 Myr. The discovery of the ~ 100 kpc 'kink' structure from our study provides an unique possibility for testing various MHD models on large scales. We have discussed few possibilities which could have lead to the creation of such peculiar structure in a dense environment. Further observations in X-rays and optical along with simulations are needed to understand this complex system better.